DOI: 10.15480/882.9316

Eighth International Symposium on Marine Propulsors
smp'24, Berlin, Germany, March 2024

Prediction of rotor sails performance on large ore carriers

Claudio Mueller Prado Sampaio[1], Kazuo Nishimoto[1], Felipe Ruggeri[2], Mariana Lopes Pinto[3], Philip von Pritzelwitz[3]

[1]*Numerical Offshore Tank, University of São Paulo, São Paulo, Brazil*
[2]*Argonautica Engineering & Research, São Paulo, Brazil*
[3]*Vale Institute of Technology (ITV), Ouro Preto, Brazil*

ABSTRACT

The application of a five in-line rotor sails system for reducing the ship's fuel consumption and, therefore, emissions was studied for a large 325,000 DWT ore carrier. The study was carried out through simulations based on Computational Fluid Dynamics (CFD), where the detailed ore carrier and rotor sails geometry were simulated and analyzed under different apparent/relative wind conditions, rotational speeds and loading conditions (laden/ballast). The simulations were carried out for a 40-years hind-cast analysis of the wind pattern along the route, with an optimization algorithm developed to obtain the optimum rotational speed for the rotor sails under each incident flow condition.

A careful evaluation of the balance between produced thrust and net required power was undertaken including the wind pattern along the route as well as several other parameters as the ship's speed, loading condition and interference among structures. Additionally, the wake interference among the set of rotor sails was also considered, as the performance depends on the true composed incident wind field.

As a result, the thrust produced by each device as well as the contribution of other structures were estimated. The net power gains of the arrangement were calculated as the cumulative probabilities of the different power gain levels showing that the final performance strongly depends on the wind pattern along the route.

Keywords: CFD simulation, rotor sails, hind-cast wind pattern, net performance optimization.

1 INTRODUCTION

The ship industry technologies have evolved appreciably in the last years looking for solutions to reduce ship's emissions/fuel consumption. Although the principles of these technologies are already known since a long time ago, there are several doubts related to the performance of these technologies in "real" operational conditions. In the case of active solutions there is an additional risk since the proposed technology requires energy to work, thus the net benefit shall be evaluated carefully to guarantee an effective emission reduction. In the case of rotor sails the performance of the system is directly related to the wind conditions that the vessel encounters during the navigation, which is also impacted by the course and speed of the ship since these variables change the relative wind condition which defines the Magnus effect thrust contribution in the advance direction. Due to the spatial and time variation of the wind conditions, it is also expected that the benefit may change appreciably for each voyage, motivating the development of a methodology to assess the expected benefit range and the overall fuel consumption reduction in a long-term operation, where several different wind conditions shall be verified.

Additionally, there are several effects in real operational conditions that are important to be considered, for instance, the shadow effects among the several structures above the deck, the rotors wake interference, the streamlines modification due to the freeboard interaction, etc. In order to evaluate these effects, Computational Fluid Dynamics (CFD) is an important tool to study the complex fluid interactions.

2 METHODOLOGY

The methodology developed to predict the performance of rotor sails in real operational conditions requires the calculation of the rotor sail net power benefit, which is obtained by computing the thrust power provided by the rotor sails in the forward direction minus the energy demanded by the device to keep the rotation, as described in Equation (1). In this equation T_{x_i} is the net thrust generated in the advance direction ($T_{x_i} = \vec{T_i}.\vec{t}$, $\vec{T}$ is the thrust vector and $\vec{t}$ is the vessel forward direction unitary vector) by rotor i, V_s is the ship's speed, ω is the rotor rotational speed, τ_i is the resistant torque and η is the electro-mechanical efficiency.

$$R_{net} = \sum(T_{x_i}.V_s - \omega\frac{\tau_i}{\eta}) \quad (1)$$

The ship's speed is an input data based on the vessel operational profile (assumed constant for simplification) and it is an important variable as the rotor thrust changes appreciably with relative wind (direction and intensity). It is computed based on Equation (2), where $\vec{V}_W(x,y,t)$ is the true wind speed at the rotor level; (x,y) the route coordinates (based on Lat/Lon values); θ_S the ship's heading (in relation to north clockwise) and t is the director vector.

$$\vec{V}_{rel} = \vec{V}_s - \vec{V}_W(x,y,t) = \\ = V_s(\sin\theta_S\,\vec{\imath} + \cos\theta_S\,\vec{\imath}) + \\ -(V_x(x,y,t)\vec{\imath} + V_y(x,y,t)\vec{\jmath}) \quad (2)$$

$$\left|\vec{V}_{rel}\right| = \left[\left(V_s\sin\theta_S - V_x(x,y,t)\right)^2 + \right. \\ \left. + \left(V_s\cos\theta_S - V_y(x,y,t)\right)^2\right]^{0.5} \quad (3)$$

$$\theta_{rel} = \cos^{-1}(\vec{V}_{rel}.\vec{t}/\left|\vec{V}_{rel}\right|)$$

$$\vec{t} = \sin\theta_S\,\vec{\imath} + \cos\theta_S\,\vec{\imath} \quad (4)$$

The rotor forces are estimated based on the relative wind intensity and direction, with the wind values corrected from the "standard" 10m wind height values by the logarithmic profile show in Equation (5) (Det Norske Veritas 2007), where z is the mean height of the rotor, computed taking into account the ship's draft (ballast and laden conditions) and ship's depth. It is to be noted that the complete wind profile was not adopted to simplify the CFD simulations convergence as described next. An additional simplification was that only the mean wind was considered, thus the gust/spectrum effect was neglected in this approach.

$$V_w(x,y,t) = V(x,y,t,10)(z\,/\,H)^{1/7} \quad (5)$$

The ship route assumed for the analysis was obtained through Satellite AIS data (Automatic Identification System) with the Lat/Lon/Heading/Speed obtained along the entire ship route as presented in Figure 1.

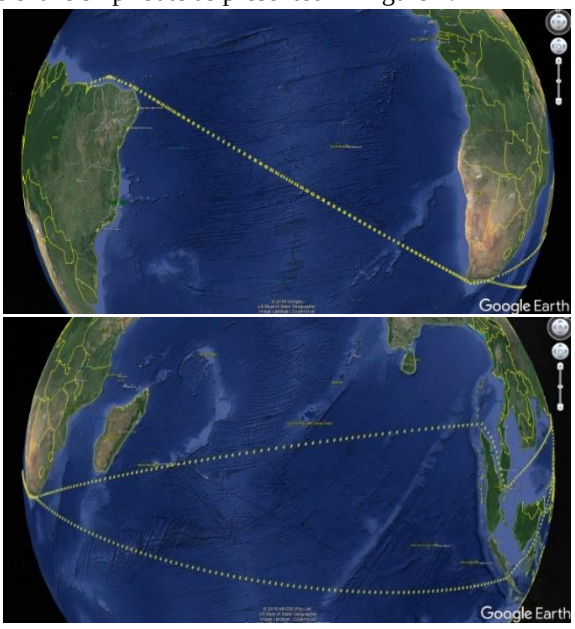

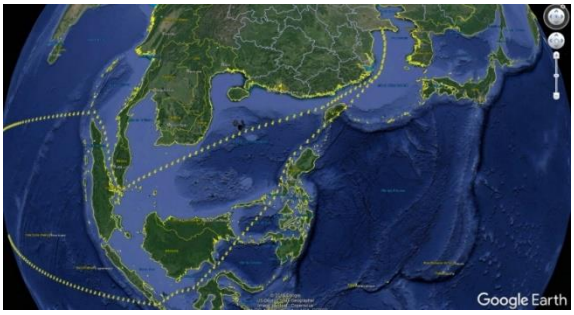

Figure 1 - Ship route assumed in the study.

The wind database was extracted from the ERA5 hind-cast model provided by the ECMWF (*European Centre for Medium-Range Weather Forecasts*) based on the 10m (u,v) mean wind components from 1979 to 2019 for the entire spatial grid. The data were interpolated at each time record to provide the wind conditions at the specific Lat/Lon along the route. An example of a wind intensity map for the entire grid during a specific timeframe can be seen in Figure 2, where the ship route is highlighted in red.

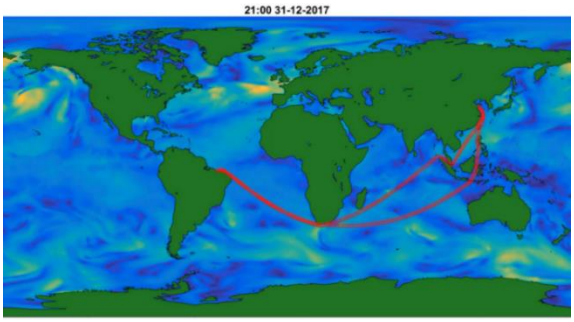

Figure 2 - Example of wind intensity map for a specific timeframe (the ship route is highlighted in red).

The wind variation (intensity/direction) range during the entire timeframe is large for each spatial position, thus the rotor sails performance shall also change drastically during the ship's service life. This wind pattern can be seen, for instance, in Figure 3, where the variation of the wind velocity in x direction, V_X (y-axis) is shown for the whole year of 1979 and the x-axis representing the navigation distance (nautical miles) along the route of the vessel during an entire round trip. In the referred figure, the gray area is the wind variation range during the year, which was split into different months to provide an idea of seasonality effects. The mean values are drawn in red, while the superior and inferior quarters are shown by blue lines.

It should be noticed that the perpendicular wind intensity along this specific route is not high as the ship's heading is not perpendicular to the east-west direction, which is the predominant wind direction in this area. This fact is extremely important because the ship's thrust diagram relies on the relative wind angle to provide a net thrust in the advance direction.

The rotor sail thrust and torque was obtained using Computational Fluid Dynamics (CFD) simulations performed using the StarCCM+ software. The vessel was modelled in detail to take into account the several non-lin-

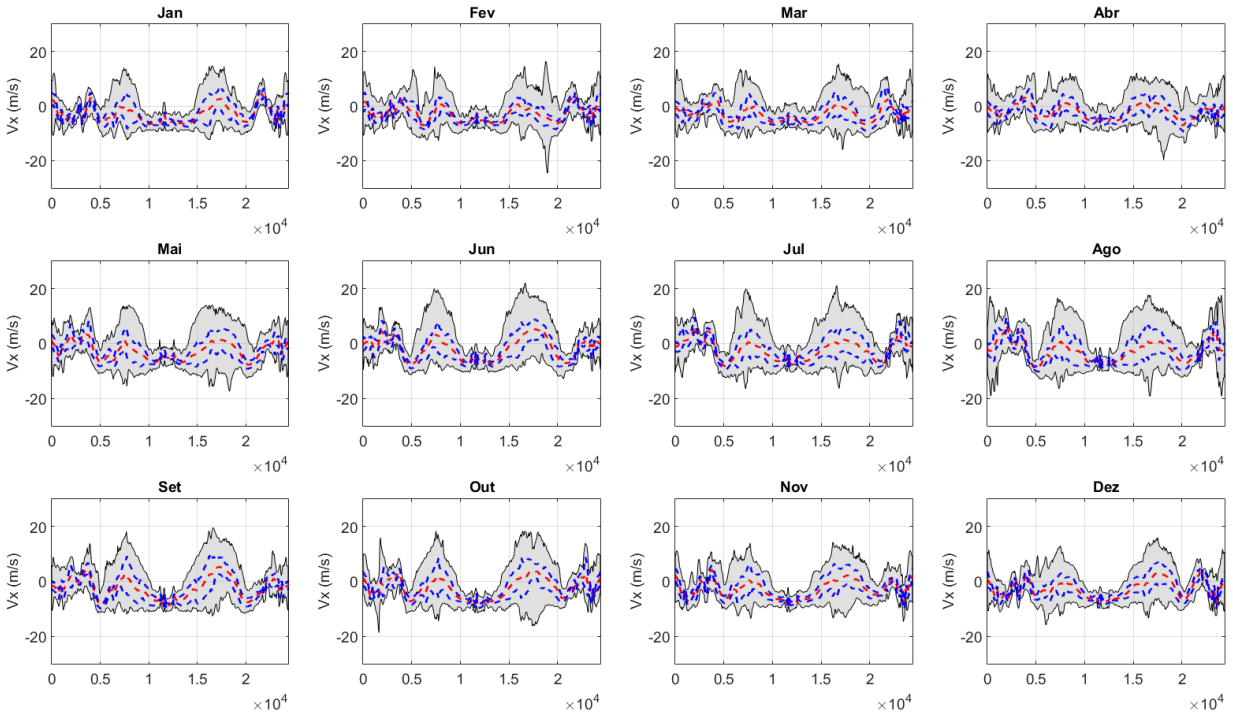

Figure 3 - Example of wind velocity in x direction, VX in several positions along the route (Lat/Lon) during the year of 1979.

ear flow effects and interactions among the rotor sails, the emerged hull side and the several deck structures such as deckhouse, hatch covers, winches, bollards, etc., see for instance, Figure 4.

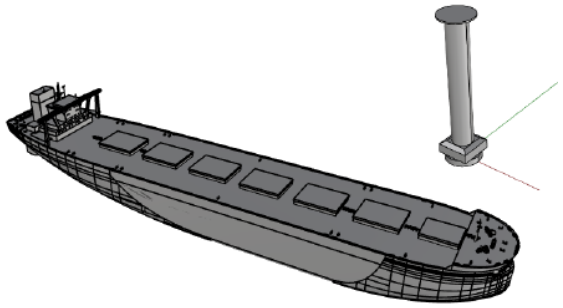

Figure 4 - Vessel and rotor sail 3D geometry.

The boundary conditions applied in the simulation are summarized in Figure 5, where the domain has a velocity inlet with a uniform wind field imposed upstream, a pressure outlet, downstream and a full slip wall condition in the bottom and lateral walls. The boundary condition on the ship hull is non-slip wall condition for the entire hull. For the rotor sails, a rotational condition is set by assuming a tangential speed boundary condition, calculated based on the rotation ω and the axis located in the center of the each rotor. This boundary condition reduces the computational effort significantly since the mesh does not need to be recreated at each time step, improving the convergence and reducing the computational effort.

Prior to begin the simulations, a sensitivity analysis was performed regarding the mesh size and domain dimensions to avoid the influence of the domain boundary conditions in the flow around the vessel as well as to reduce excessive computational resources. A systematic variation procedure was performed to establish a reasonable robust domain of five LOAs (*Length Over All*) in length directions (1 LOA windward and 3 LOA leeward), 5 LOAs width and 150m height.

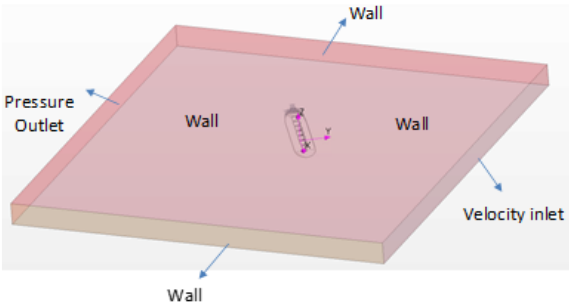

Figure 5 - Boundary conditions applied in the CFD simulations.

The ship is located in the origin of the domain and is rotated to simplify the automatic simulation procedure, with a script created to rebuild the mesh, change the wind conditions and perform the simulations, allowing a systematic variation. Additionally, a local axis is adopted to deliver the thrust forces, generated by the rotor sails, directly into the ship's advance direction.

The original built mesh had about 18 million elements due to the refined discretization of the ship above water hull structures, as shown in Figure 6, where the large complexity of deck arrangement is observed. In order to reduce the mesh size, the different elements were grouped into similar contributors and preliminary simulations were performed to estimate their individual contribution to total wind force acting on the above water hull. Based on these simulations, it could be verified that winches, bollards,

anchors, mast and other small parts were responsible to less than 0.37% of the total drag, with their wind field influence locally restricted.

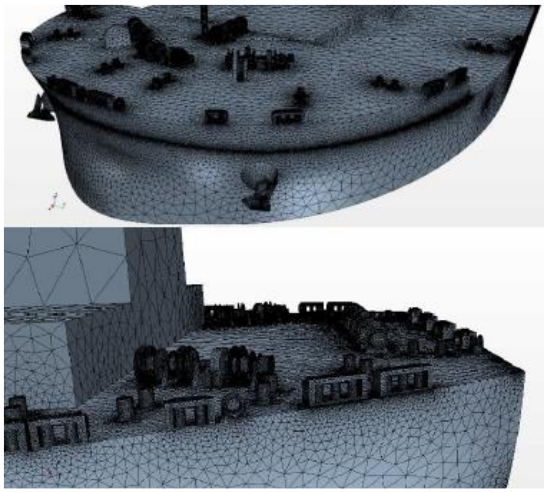

Figure 6 - Details of the ship's surface mesh.

These elements were therefore removed from the discretized mesh while keeping the deckhouse and the hatch covers, which provide most of the resistance and interference effects. This procedure allowed the reduction of the final mesh to a range between 10-12 million elements depending on the relative wind direction, which is considered adequate for a 3D model. The influence of the deckhouse and the hull side (freeboard) in the wind field was verified to be not negligible as observed in Figure 7.

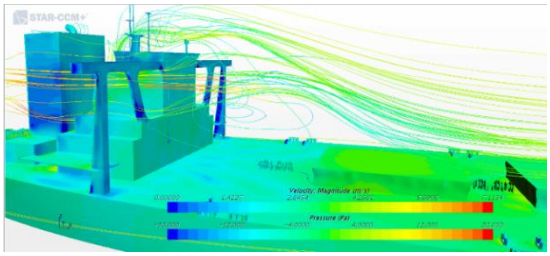

Figure 7 - Example of deckhouse influence in the wind field.

Since the rotor sails arrangement was symmetrically distributed in the ship, the relative wind directions simulated were in the range of 0 to 180º (22.5º increment) considering the OCIMF (OCIMF 2018) wind direction definition illustrated in Figure 8. Besides, as the vessel structures were also approximately symmetrical, the eventual small asymmetries were neglected to reduce the number of simulations.

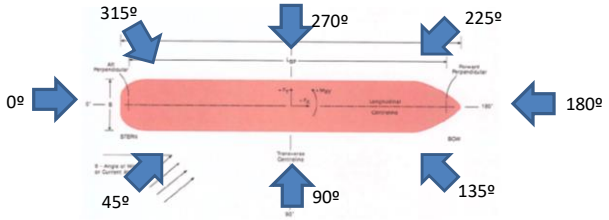

Figure 8 - Wind direction definition.

The simulations were performed for relative wind speeds of 2, 5, 10, 15, 20 and 25m/s, which covers almost the entire range of relative wind speeds expected for the operational conditions. Furthermore, as the optimum rotations were not known in advance, the values of 50, 100, 150 and 200 rpm were also assumed for the simulations and, although in practice the rotations may change individually for each rotor sail, in the study they were assumed equal to simplify the analysis.

As iron ore has a large density, the vessel draft significantly changes between the cargo deliver voyage (laden condition) and return voyage to the export port (ballast condition), as illustrated in Figure 9. These two conditions were included in the simulations to verify the impact of the freeboard into the incident wind field acting at the rotor sails. The simulations were performed in steady state, neglecting eventual transient effects.

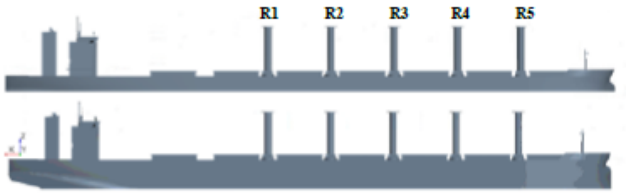

Figure 9 - Ore carrier model considering the laden and ballast conditions.

Since the optimum rotation of the system was unknown and increased rotations demand more torque (increasing energy to keep the device working), an optimization algorithm was created and applied for each route position and wind incident condition. As summarized by the objective function shown in equation (6) and the constraints given by equations (7) and (8), these were obtained directly from the device manufacturer based on the maximum rotation allowed to avoid excessive vibrations as well as on structural design limitations due to the bending moment on the device footing structure. Besides, due to electrical power balance of the vessel, an additional constraint (9) was included based on the maximum power (energy) allowed for the device operation.

$$\max_{\omega} \sum(T_{x_i}.V_s - \omega\frac{\tau_i}{\eta}) \quad (6)$$

with: $-\omega_{lim} \leq \omega \leq \omega_{lim}, i = 1,2,\dots 5$ (7)

$$0 \leq \left[T_{x_i} + T_{y_i}\right]^{0.5} \leq T_{MAX}, i = 1,2,\dots 5 \quad (8)$$

$$0 \leq \omega\,\tau_i(\omega)/\eta \leq P_{MAX}, i = 1,2,\dots 5 \quad (9)$$

Since it is not possible to establish in advance the probability of a vessel passing a specific point of the route for the wind conditions. The "average" benefit is computed based on Eq. (10), where R1 and R2 are the routes in ballast and laden conditions and P (V_{rel}, θ_{rel}) is the probability density function of the relative wind and R_{net} is the net benefit obtained from the optimization algorithm. For each specific point of the route there is a probability density function of the absolute wind conditions, which is combined with the ship's speed to provide the relative wind speed distribution.

$$\int_{R_1} P(V_{rel}, \theta_{rel}).R_{net}(V_s, T_{ballast}, V_{rel}, \theta_{rel})\,dP +$$

$$+\int_{R_2} P(V_{rel},\theta_{rel}).R_{net}(V_s,T_{laden},V_{rel},\theta_{rel})\,dP \qquad (10)$$

The proposed methodology can be summarized as shown in Figure 10, which was converted into a numerical code called "*RotorSim*".

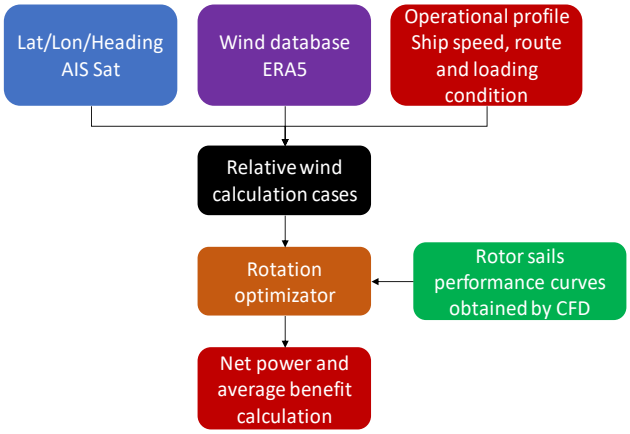

Figure 10 - Summary of the proposed methodology.

3 CASE STUDY

The proposed methodology was applied to a large ore carrier operating in the route from Brazil to China and Singapore. The vessel main dimensions are given in Table 1 while the rotor sails dimensions are 4.0m diameter (main part), 24.2m height and tip diameter of 6.6m.

Table 2 - Vessel main dimensions.

LOA (m)	340.0
Lpp (m)	333.1
Beam (m)	62.0
Depth (m)	29.5
Laden draft (m)	21.4
Ballast draft (m)	13.0

The ship's heading distribution diagram is shown in Figure 11, where it can be noted that the heading is predominantly in the east-west direction when compared to the south-north one. Finally, for this case study, the simulations are performed considering two SOGs *(Speed Overground)* of the ship that is 7.5 and 15 knots.

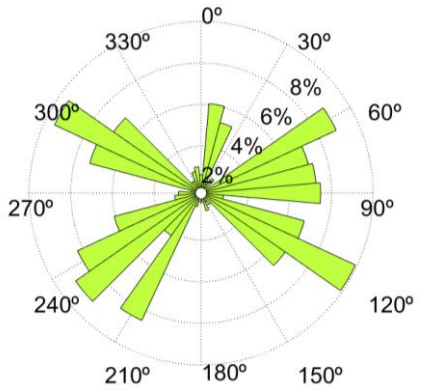

Figure 11 – Ship's heading distribution diagram along the navigation.

4 RESULTS

The CFD simulations were performed for the different wind conditions previously presented as well as for both laden and ballast conditions (21.4m and 13.0m drafts). It is important to note that the freeboard corresponds to an obstacle for the incident wind into the rotor sails and, depending on the wind intensity, a large flow separation can occur, modifying the incident flow into the rotor sails significantly, with greater interference when in ballast condition due to the additional 8.4m of freeboard.

An illustrative example of the flow stream and pressure and velocity fields around the hull can be seen in Figure 12 for an incidence angle of 270º (beam condition), relative wind speed of 20m/s and rotor sails at 200 rpm, in which large additional effects on the wind turbulence around the deck can be observed for the ballast case.

An additional example of the flow effects on its incident direction is shown in Figure 13 where three incident relative wind directions (292.5º, 347.5º and 360º) are given. In these cases, specifying the z component of vorticity, it can be observed that there is a major wake interference on the incident flow of each particular rotor sail, this interference depending on the incident wind direction. Besides, as already commented, these effects are intensified in the ballast condition. Finally, for the 360º case, that is following winds, the deckhouse interference has major contribution on the incident rotor sails flow, with minor effect of the ship's loading condition.

The longitudinal forces acting in each structure were exported to quantify the contribution of each rotor in terms of longitudinal force as well as of the other elements of the ship's structure (e.g: deckhouse, hatch covers etc). An example can be seen in Figure 14 for a fore to beam (202,5º) and beam to aft (315,0º) relative incident angles under a 10 m/s relative wind intensity and 200 rpm rotor sails rotation. The red bars represent the force in x direction from the deckhouse and the hull, the green bars provide the contribution of each rotor sail and, finally, the blue bar corresponds to the total longitudinal force considering others elements not included in the chart (hatch covers, forecastle, etc.). Negative values correspond to additional resistance to the advance move of the ship, while positive ones correspond to thrust in the forward direction.

The results in the diagram also indicate that for small angles of incidence from aft to beam (less than 30º from the centerline), the contributions are quite significant with the rotors having high efficiency and the deckhouse and the hull also having major contributions. In the case of incidence by the bow (202.5º) the rotor sails near the bow region (R4 and R5) show good efficiencies due to the smoother incident flow in spite of the forecastle, while the other rotor sails, located further aft, have a very disappointing performance because of the interference among rotors' wakes and the deckhouse effect on the flow.

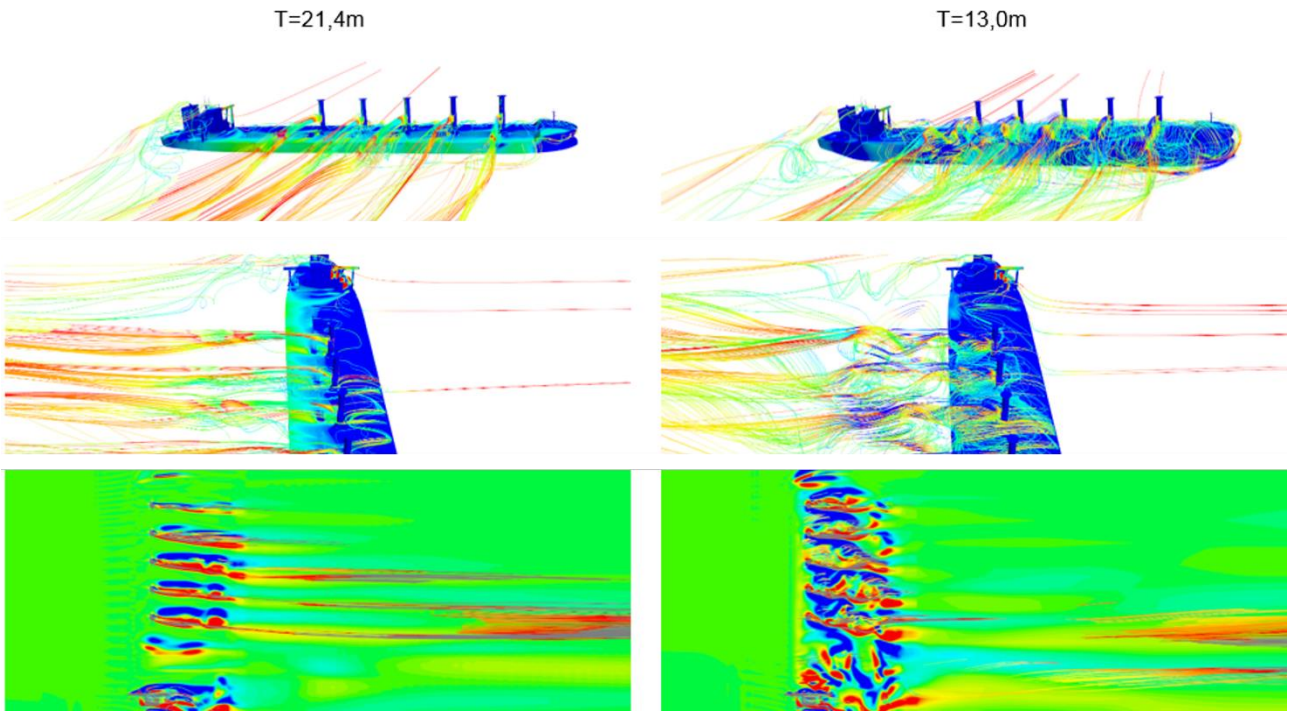

Figure 12 - Example of flow stream, velocity, pressured and vorticity fields in laden (left) and in ballast (right) conditions for a relative incident wind angle of 270º with a 20 m/s speed.

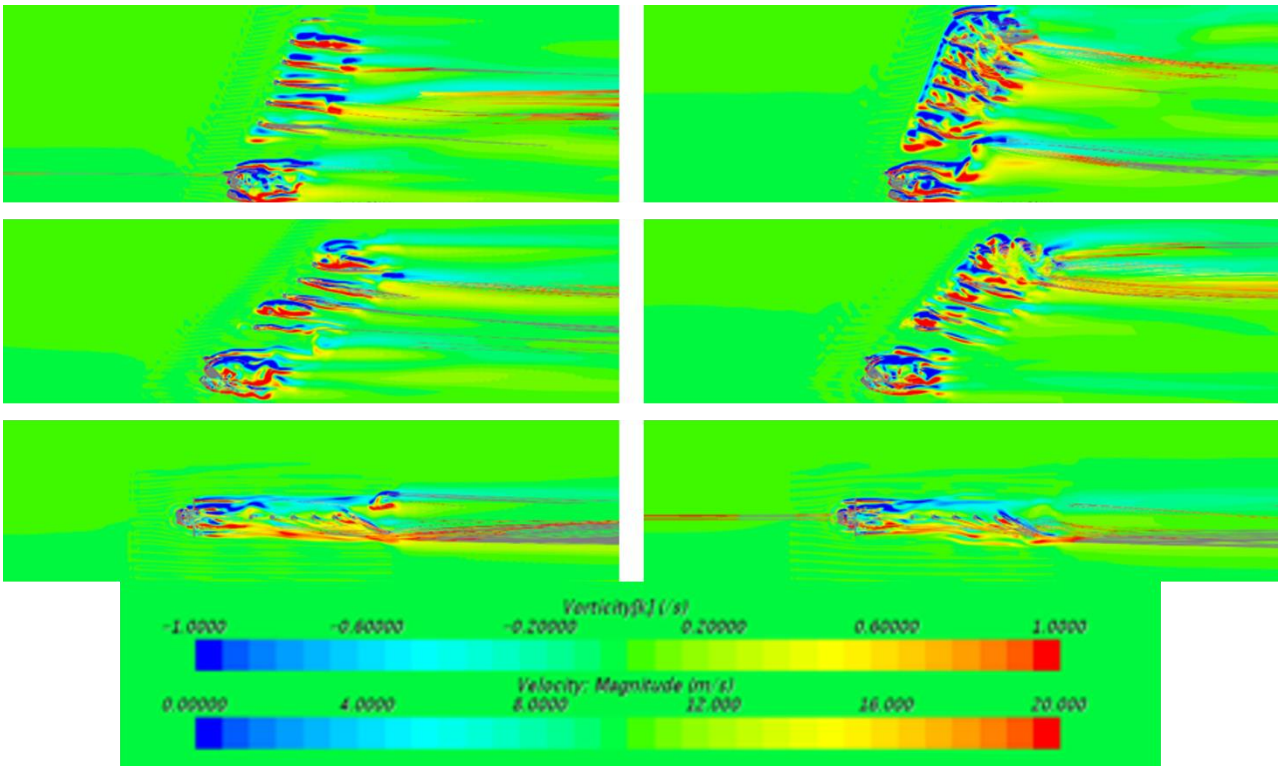

Figure 13 - Vorticity z for laden (left) and ballast (right) conditions for relative wind directions of 292.5º, 347.5º and 360º.

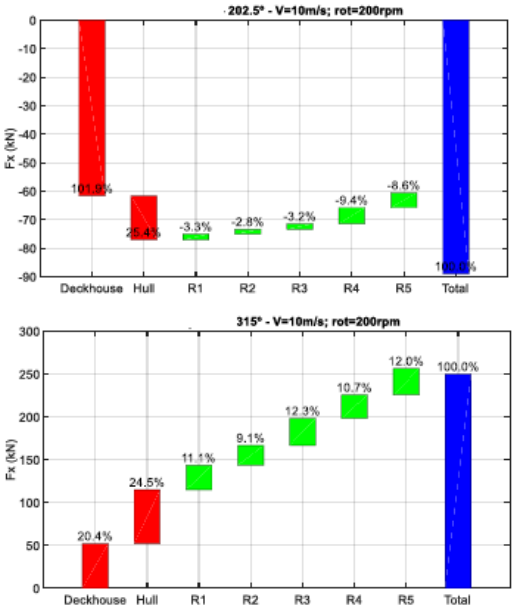

Figure 14 - Breakdown of the thrust force generated by the rotor sails, deckhouse and hull for different relative angles.

It may be verified that by stern incidences, the closer to the beam direction, the larger the intensity. In these cases the rotor sails' contributions tend to be of the same order of magnitude because the smaller interference among the wakes and therefore the smoother incidence flow at each individual rotor sail. On the other hand, the deckhouse and the hull have a decreasing effect on providing additional thrust as it would be expected.

Figure 15 shows an example of the freeboard effect into the rotor sails performance that is, for the full and ballast conditions. This evaluation corresponds to the extreme situation of a relative beam wind incidence, with an assumed relative velocity of 10m/s and rotor sails under a 200rpm rotation. This particular condition represents the situation of the largest rotor sails efficiency, the rotor sails having similar contributions in terms of longitudinal force (less effects of wake interference).

Analyzing the results, the thrust provided by each rotor sails in both conditions are similar but, in the ballast condition all values are smaller than in the full load condition because the incident flow encounters a larger barrier (freeboard) to overcome. In the results presented, it is interesting to note that the hull itself contributes to the longitudinal thrust, in the ballast condition almost twice when compared to the loaded one, a fact that results from the larger freeboard. The force generated in the longitudinal direction represents essentially the asymmetries between bow and stern regions, which change the pressure field around the hull combined to the exposed windage area.

In order to summarize the contributions of the rotor sails as a function of the relative wind conditions (speed and incident angle) and rotation, several diagrams were generated, as illustrated in Figure 16, in which the colors represent the velocities and the markers the two assumed rotations. Besides, the dashed and continuous lines represent, respectively, the laden and ballast conditions; the x-axis representing each rotor sail.

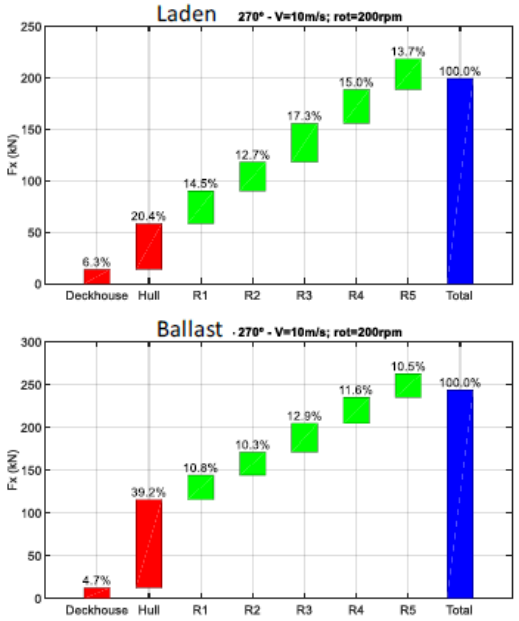

Figure 15 - Breakdown of the thrust force generated by the rotor sails, deckhouse and hull for laden and ballast condition under a 10m/s beam relative wind condition.

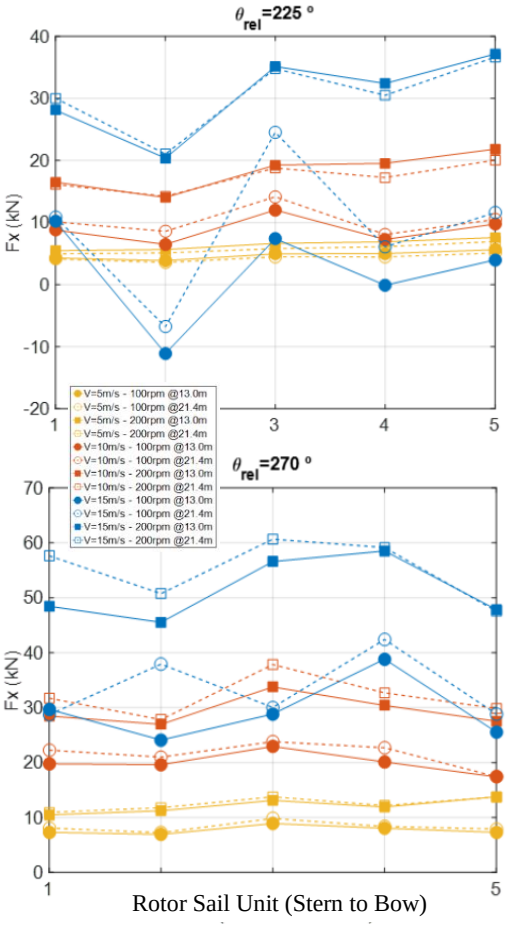

Figure 16 - Thrust generated by each rotor sail for different rotations and relative wind speeds for 225° and 270° relative incident angle.

The figure shows that the higher rotational speed provides a better performance whatever the wind incident speed, which itself also increases the efficiency of each rotor-sail. The laden condition has a better performance due to the smaller perturbation generated by the freeboard. Finally, it is interesting to note that there is some oscillatory pattern in the thrust provided by different rotor-sails probably due to the interferences among them, one specific case showing negative thrust, although the total thrust still positive.

Continuing the development of the optimization algorithm, it was decided to implement a thrust diagram routine for a better understanding of the rotor sails contribution based on the ship's forward speed in which the intensity and direction of the absolute wind is converted to relative wind conditions. In Figure 17 the thrust diagrams are presented for three navigation speeds, 0, 7.5 and 15 knots considering the rotation that provides the maximum overall thrust and the dashed and solid lines corresponding, respectively, to ballast and laden conditions; the radii, the force intensity in the x direction with wind directions following the OCIMF (OCIMF 2018) convention. Finally, the results for different absolute wind speeds are identified by colors.

It can be noticed (Figure 17) that the higher efficiencies are observed for incidence from aft to beam direction, the best incidence angle depending significantly on the navigation speed that compose the relative velocity vector. Besides, it is also interesting to observe that as the advance speed increases, the most effective thrust (x-direction force) decreases in intensity (vector sum of the lift and drag components) while the butterfly graph moves backwards, that is the wind incidence occurring more from the aft. It can also be verified that, the lower the incident wind speeds, the less effect of the ship's advance speed in reducing the thrust from bow incident winds, this behavior seen in the diagram for cases till 11m/s.

These thrust diagrams were combined with the wind database for the whole obtained records (between 1979 and 2018) into the optimization algorithm in order to obtain for each route node the net power produced by the rotor. It was assumed, for this purpose, a homogeneous probability distribution for time and space that is the probability of the vessel being at any route node is the same. This simplification aims to avoid the complexity of correlating the exact moments of the ship's passage through a certain location thus transforming position and time into random variables with uniform distribution.

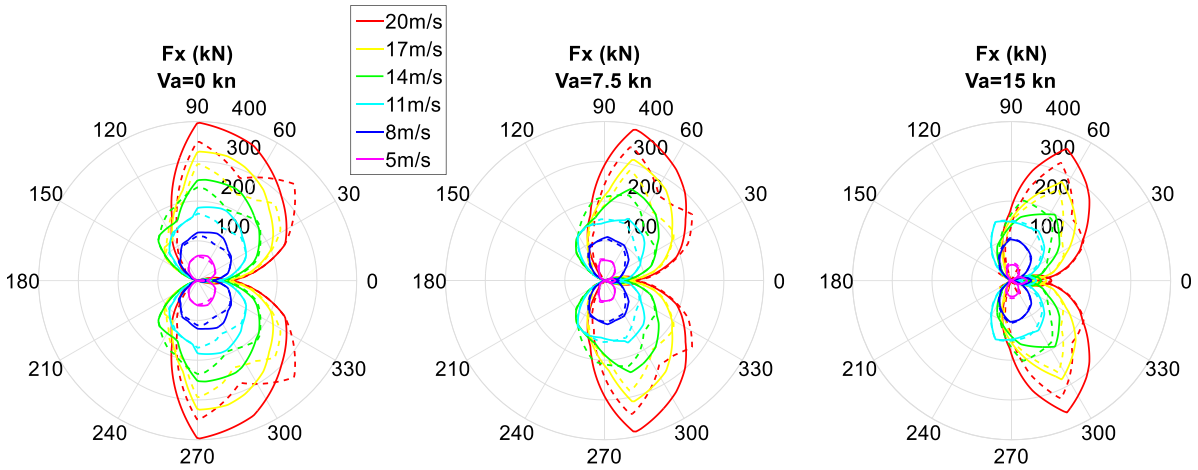

Figure 17 - Rotor thrust diagrams for 0, 7.5 and 15 knots of the ship's advance speed.

For each simulated year, maps of the total thrust per rotor were produced, the use of the maps turning possible to identify the points on the route with the most favorable winds, as well as to observe the large variation of the thrust forces produced by the 5 rotor sails system over time. Besides, by this procedure it was also possible to verify the most favorable wind condition for the navigation (wind coming from the aft to beam direction) which in the example occurs at the change of direction occurring around Singapore.

These maps, however, change appreciably according to the year and to the navigation speed so that the results over the entire time series and all route positions (nodes) were put together into a probability distribution of the rotor power reduction. The summarized results are shown in Figure 18 where cumulative probabilities are given for loaded and ballasted conditions under 10 (blue) and 15 knots (red) navigation speeds.

It can be seen that there is a large variation in the net power produced by the set of rotor sails, a fact that is directly related to the variation of wind conditions along the route. As illustrated, the power net production up to 500kW has a probability around 25% for the laden condition while, for the ballast condition, for the same range, the probability corresponds to 17%. Besides, it is to be noted that, for net powers over 500 kW, the effect of the full load condition is such that there is a larger probability of higher gains in net power production at higher speeds than in the ballast condition. Also in an extreme case, if there are no operational limits on the system, net reductions up to 4000 kW for ballast conditions could be obtained although these very favorable wind conditions are extremely rare.

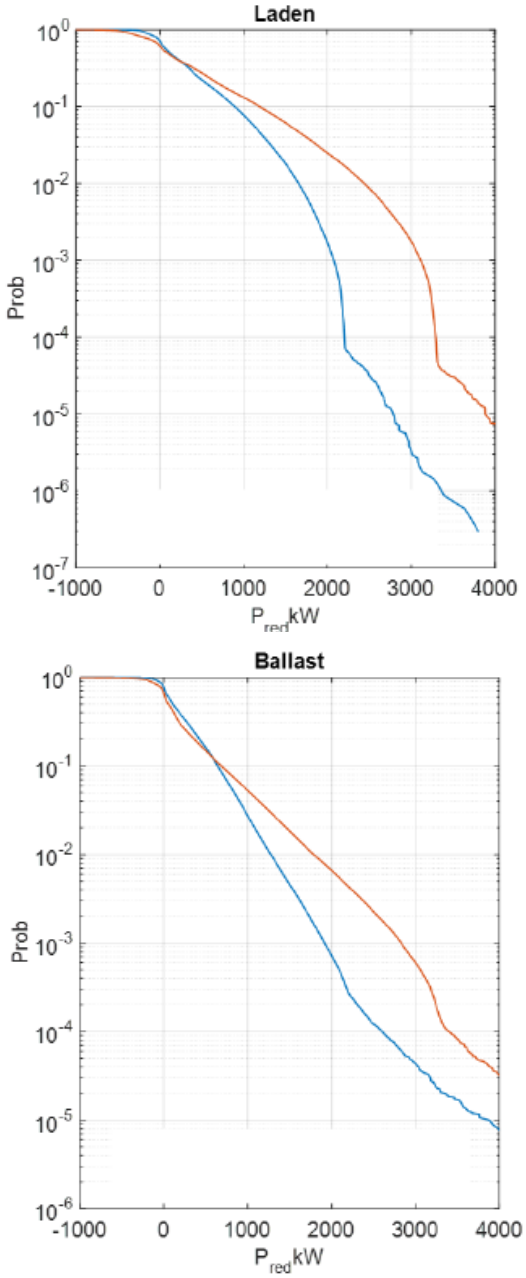

Figure 18 – Rotor sails produced net power probability function in laden and ballast conditions at 10 knots (blue) and 15 knots (red) speeds.

Finally, it can also be observed that there are some cases in which the net power reduction is negative, that is, an increase in consumption along the voyage, a fact that results from the rotor sails working as an additional drag element independent of its rotation. In such situations, it is recommended not only to turn off the rotor sails, but also to tilt them down, if possible.

4 CONCLUSIONS

This paper presented a methodology to predict the performance of rotor sails in real operational conditions for a specific large vessel in a specific route. It was observed that the rotor sails performance in the route Brazil to China change appreciably in space and time, as verified in a 40 years hind-cast analysis, which indicated a significant variation in both intensity and direction.

The CFD simulations were applied to obtain the performance of the rotor sails considering the several interactions among rotors and other structures of the ship (deckhouse, hatch covers, etc.). This procedure demonstrated that the rotors performance are not homogeneous in most conditions due to the complex flow interactions, where the incident wind is not undisturbed and homogeneous for the rotor sails with a large influence of the deckhouse (mainly for aft incidence conditions) and the freeboard (mainly in the ballast condition). In some specific cases, one of the rotor-sail may produce almost 4 times more thrust than another one due to these interaction effects. The thrust diagrams also demonstrated the variation of the net thrust according to the advance speed, which turns the analysis even more complex since it also changes the relative wind incidence condition.

By considering a uniform probability density function for the wind conditions in space and time during the 40 years period, the simulation allowed to verify a large variation in performance of the rotor sails. In some cases almost no generating net thrust (or even negative values in some specific conditions) was produced while in other conditions, the thrust generation showed a very meaningful additional thrust/net power reduction, therefore highlighting the importance of including the expected wind regimes along the route into the analysis.

ACKNOWLEDGMENT

The authors gratefully acknowledge VALE Technological Institute (ITV) and VALE S/A for the technical-financial support provided during this research.

REFERENCES

Det Norske Veritas (2007). Recommended Practice DNV-RP-C205 - Environmental Conditions and Environmental loads.

OCIMF (2018). Mooring Equipment Guidelines, MEG4.1 (4th Ed.).